LA-UR-07-6876

Initial Mechanical Stability of Cementless Porous Titanium Porous Titanium Patellar Components Using Micromotion and Vibration Analysis

R. Parker Eason[1], Noah Ledford[2], Tarisa Lerro[3], Phillip Cornwell[4], Philip Rae[5], R. Ben Willms[5], R. Michael Meneghini[6], Arlen Hanssen[7]

[1] University of Maine, Orono, ME 04469
[2] University of Missouri Rolla, Rolla, MO 65401
[3] University of Wisconsin – Milwaukee, Milwaukee, WI 53201
[4] Dept. of Mechanical Eng., Rose-Hulman Inst. of Technology, Terre Haute, IN 47803
[5] Materials Science Group, Los Alamos National Laboratory, Los Alamos, NM 87545
[6] St. Vincent Center for Joint Replacement
[7] Mayo Clinic Department of Orthopaedics

ABSTRACT

Cementless fixation in total knee replacement has enjoyed limited success in the past; however, there is a renewed interest in cementless fixation, which has the potential to increase operative efficiency and to improve the strength of the bone-implant interface. The initial mechanical stability of cementless implants is critical to minimizing micromotion between the bone and the porous-coated surface, thus providing the necessary conditions for successful osseointegration (long-term bonding between the bone and implant). A critical element to any total knee replacement system is a durable and well-functioning patellar component. The first purpose of this study is to assess whether vibration analysis techniques can be used to evaluate and characterize initial mechanical stability of cementless implants as accurately as the traditional method of micromotion measurement using LVDTs, which have significant experimental limitations. The second purpose is to evaluate and determine the comparative mechanical stability of various designs of cementless patella components under mechanical loading designed to simulate *in vivo* forces. The various designs included two control groups of cemented patella designs; a "cementless control" of a currently accepted cementless design; a group of newly-developed, cementless, porous titanium designs; and a cementless design with oversized peg holes. The LVDT data showed no statistical difference between the two cemented groups, nor between the press-fit cementless groups, although the cemented groups had less micromotion than the uncemented groups. Vibration analysis techniques were not able to accurately assess mechanical stability.

1 INTRODUCTION

1.1 Background

Total knee replacement (TKR) arthroplasty involves substitution of worn-down bone and cartilage with implants designed to withstand the *in vivo* (in the body) forces. This surgery requires long-term bonding between the bone and implant, or *osseointegration*. Improper fixation or bonding of the implant to the bone may lead to artificial joint failure and potentially additional surgery. This bonding has been traditionally provided with cement, as cementless designs have had higher failure rates in the past than cemented designs [1].

1.2 Motivation

Recent studies in cementless prosthetic attachment TKR surgery have investigated the femoral [1] and tibial [2-4] components. There is a need to study the mechanical stability of a cementless patella design. Cementless TKR eliminates operative time normally needed to allow for the cementation and curing processes, effectively

minimizing the risk of infection. Cement also produces an additional interface with failure potential. Previous metal-backed cementless designs had high failure rates, but newly-developed porous titanium designs have improved interfaces to support long-term fixation through osseointegration.

Successful osseointegration requires minimal micromotion between the implant and the bone. Previous studies show that micromotion greater than 150 μm leads to fibrous tissue development on the bone-implant interface, interfering with successful osseointegration [5-24]. Micromotion less than 40 μm provides the stability needed for osseointegration [25-28].

1.3 Purpose

This study had two objectives. The first goal was to evaluate the micromotion associated with six sets of patellar implants designed to simulate post-operative *in vivo* loads. These designs varied in peg structure, peg hole size, fixation methods, and material composition.

The second goal was to compare traditional micromotion tests using linear variable differential transducers (LVDT) to methods using vibration analysis. LVDTs have experimental limitations, partly due to the fact that it is often difficult to create a reliable experimental construct with LVDTs to measure relative displacement between all three orthogonal directions.

Three vibrations tests were performed using piezoelectric transducers (PZTs). A baseline was measured before the loading cycle, and data was recorded for comparison between loading cycles and after the second loading cycle. A white noise excitation was used as the input when determining frequency response functions (FRFs). These FRFs also provided the basis for reciprocity tests, which checked the linearity of the system as the testing progressed. The PZT sensors again excited the structure with white noise to produce data to form an impedance spectrum. Changes in the measured electrical impedance have been shown to be directly related to changes in the mechanical impedance of a structure [29].

2 EXPERIMENTAL PROCEDURES

2.1 Test Sample Preparation

There were six groups of patella samples to be tested, which were distinguished as shown in Table 1:

Table 1: Acronyms and descriptions for each patella group

CON	Cemented all-polyethylene patellae (cemented control group)
MBC	Cemented metal-backed (chromium beads) patellae with a white peri-apetite coating to replicate the chemical composition of bone; cylindrical pegs
PCC	Cementless control group (chromium beads) with a peri-apetite coating; cylindrical pegs; press fit
PCL	Similar to PCC, but with a loose fit (oversized peg holes on block)
CPF	Cementless group (porous titanium beads); also has 1 mm boss designed to sit in 1 mm inset in bone foam
HPF	Similar to CPF, but with hexagonal pegs instead of cylindrical pegs

The test schedule was randomized to reduce systematic error. All patellae were impacted by an orthopedic surgeon using an impactor. This allowed for a consistent impaction and simulated the surgical procedure as closely as possible.

One area of concern was the gap between the patella and the bone foam in the CPF and HPF groups. As noted in

Table **1**, these two groups were designed to be seated in a one millimeter circular inset pocket in the bone material, allowing the bottom of the patella to lie flush with the bone surface, as shown in Figure 1. This was designed to distribute shear from the pegs to the entire metal-backed surface. However, the polyurethane foam blocks did not have this inset, causing a gap to form as shown in Figure 2, potentially altering the performance of those patellae under loading.

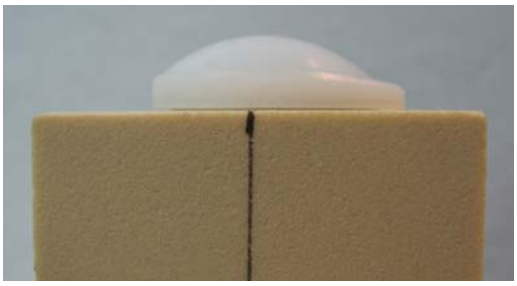

Figure 1: Correctly seated patella in bone foam

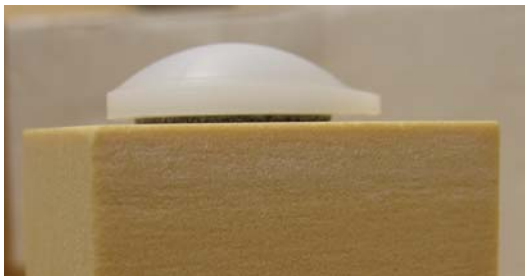

Figure 2: Gap between patella and bone foam

Two PZT patches were attached to each sample. Figure 3 shows the approximate PZT patches' locations. The FRF tests required the two PZT patches, while the impedance tests required only one self-sensing-actuator. Both patches were used, however, to collect two sets of impedance data. The sensor locations were selected to maximize signal output quality based on preliminary experimental tests.

The surfaces on the bone foam were sanded and cleaned to maximize adhesion of the PZT patches. The sensor on the patella was more challenging to attach due to the curved patellar surface seen in Figures 1 and 2. The quality of the bond was confirmed by examining the imaginary part of the impedance measurements, which has been shown to indicate bond quality [29].

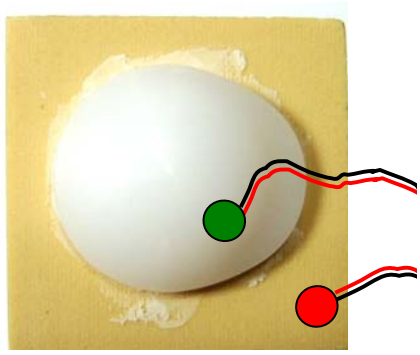

Figure 3: Location of PZT patches on patella

2.2 Test Methodology and Remarks

2.2.1 Linear Variable Displacement Transducer (LVDT)

The LVDT tests were the only tests that produced quantifiable micromotion results. The information gained from these tests allowed the most direct micromotion comparison between different patellar designs.

To perform the LVDT test, Los Alamos National Laboratory (LANL) and Stryker Orthopaedics collaborated to design and construct a custom setup as shown in Figure 4. Stryker provided the components to attach the LVDTs to the bone foam, which were installed at LANL. A schematic of the test setup is show in Figure 5, which shows the adjustment plates used to ensure consistent loading application on the samples, regardless of varying patellar position or orientation. This test structure was designed to allow the load to be applied at an angle that simulated both the *in vivo* shear and compression forces experienced by the patella. The angle was selected to resolve the applied force into an approximately 800 N compressive force and a 270 N shear force. The test structure also made it possible to adjust the samples so that each one had consistent boundary conditions.

Figure 4: Test setup

The LVDT measurements were taken during two loading cycles designed to simulate forces resulting from squatting and walking, respectively. Both loading cycles consisted of 60 cycles of loading that varied sinusoidally from 50 N to 850 N. The first cycle was at a 0.2 Hz frequency, and the second was 1.5 Hz.

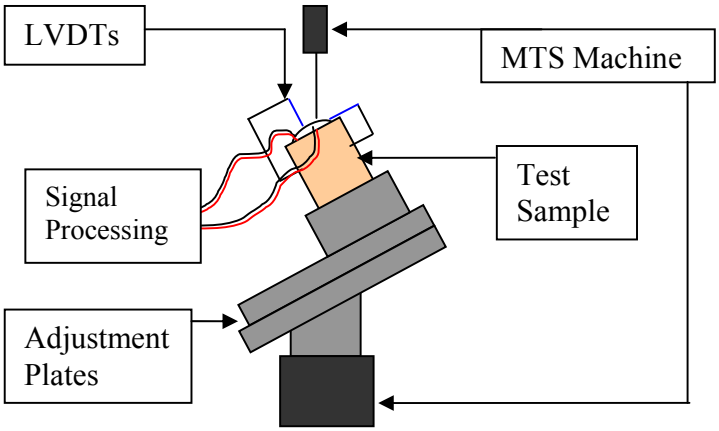

Figure 5: Schematic of LVDT setup

2.2.2 Frequency Response Function (FRF)

The results from a number of vibration analysis techniques were compared to the micromotion found from LVDT tests. The FRF test used one PZT patch to excite the structure with a burst random signal and the other PZT patch to record the structural response. Tests were performed at different points during the loading sequence so that changes in the system, such as micromotion between the patella and the bone foam, may be observable.

2.2.3 Impedance

As mentioned earlier, the change in electrical impedance of a PZT transducer is directly related to changes in mechanical impedance of a structure. Therefore, this quantity can be used to determine if there has been a change in the system. High frequencies (in the range of 100 kHz to 190 kHz) were used to excite the structure. High frequencies are more sensitive to small defects in the region of the PZT than low frequencies

2.2.4 Reciprocity

Reciprocity is a characteristic of a linear system. Given two PZT patches, a linear structure should exhibit the same responses to excitation independent of which PZT patch acts as a sensor and which acts as an actuator. The linearity of a structure can be assessed by finding the FRF using one configuration, then reversing the PZTs' roles while otherwise maintaining the same experimental conditions and repeating the measurement. Damage, or other nonlinearities, should be reflected by the corresponding signals exhibiting less reciprocity.

2.3 Data Analysis Techniques

2.3.1 Linear Variable Displacement Transducer (LVDT) Analysis

The LVDT data gave the patella position relative to the bone foam as a function of time, from which the maximum relative displacement could be found. The metrics used to compare data were the average displacement and standard deviation for each patellar group.

An analysis of variance (ANOVA) test was used to determine whether displacement differences between the sample groups were statistically significant. The null hypothesis in each case was that there was no difference between the groups, with a significance level of 0.05.

2.3.2 FRF Analysis

The FRF data was acquired before, after, and in between the two loading cycles. Each FRF used the green PZT patch as an actuator, and the red as a sensor, as shown in Figure 3. These three FRFs were compared to each other using two methods: the frequency response assurance criterion (FRAC) and the normalized cross-correlation. The FRAC is a scalar-valued normalized dot product, computed as shown in Eq. 1.

$$\mathrm{FRAC}(f,g)=\frac{\left|f^{\mathrm{T}}\cdot g^{*}\right|}{\left[f^{\mathrm{T}}\cdot f^{*}\right]\left[g^{\mathrm{T}}\cdot g^{*}\right]} \tag{1}$$

where f and g are column vectors of the signal data Theoretically, the closer the FRAC is to unity, the less the change in the signal being examined. Although the FRAC can be used to compare complex quantities, and the FRF is a complex quantity, only the magnitude of the FRF was used in the FRAC calculations in this study.

The normalized cross-correlation is a vector-valued function for discrete data sets as given by Eq. 2

$$\mathrm{xcorr}(f,g)_i = \frac{\sum_j f_j^* g_{i+j}}{\left[f^{\mathrm{T}} \cdot f^*\right]\left[g^{\mathrm{T}} \cdot g^*\right]} \tag{2}$$

where, again, f and g are column vectors of the signal data. The signals were normalized so that the maximum values of their respective auto-correlations were equal to one. The maximum value in the cross-correlation vector was the metric used to quantify the difference between signals.

2.3.3 Impedance Analysis

The impedance data was analyzed using the FRAC and cross-correlation methods discussed in Section 2.3.2. Like the FRF, the impedance profile was found before, after, and in between the loading cycles. These three profiles were again compared to each other using the FRAC and normalized cross-correlation.

The real part of the impedance was used in the FRAC and cross-correlation calculations, because research has shown that structural damage causes changes to the real impedance [29]. The shape and slope of the imaginary impedance curve reflects sensor and bonding quality. The imaginary part of the impedance data indicated that the PZT patches were bonded well to the patella and simulated foam throughout the entire testing procedure.

2.3.4 Reciprocity Analysis

Data from the reciprocity tests were analyzed using the FRAC method discussed in Section 2.3.2. Two FRFs were taken as described in Section 2.2.3 at three points during the loading sequence. Unlike the FRF analysis, which measured the FRACs of the FRFs between different points in the loading cycles, the reciprocity tests measured the FRACs of the two FRFs taken at the same point in the loading cycle. The linearity of the structure, and therefore the FRACs, was expected to decrease as the testing progressed.

3 RESULTS

3.1 LVDT Results

Figure 6 shows the maximum displacement for each loading cycle by group. From this figure, it appears that there is very little difference between the average magnitudes of the CON and the MBC group, and, similarly, very little difference between the average magnitudes of the CPF, HPF and PCC groups.

The values for cemented groups CON and MBC averaged about 29 μm of displacement during the first loading cycle with standard deviations of 6.2 μm and 8.3 μm, respectively. The cementless groups CPF, HPF and PCC displaced an average

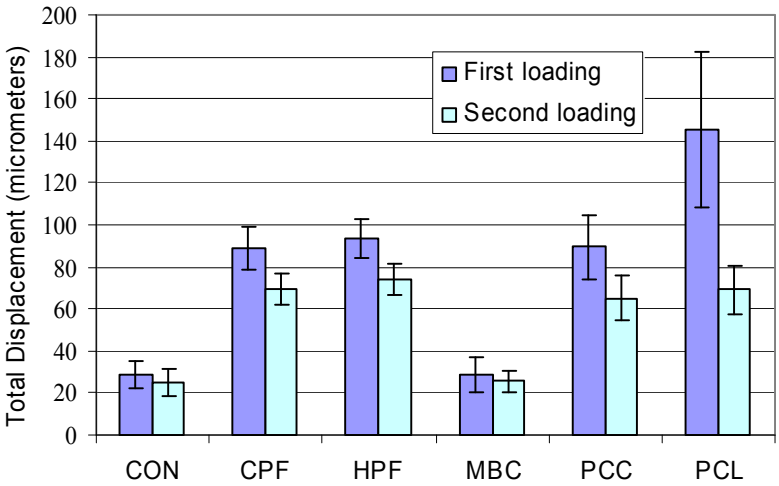

Figure 6: Average magnitudes from each loading cycle by group

of 90 μm with respective standard deviations of 10.3 μm, 9.2 μm and 15.4 μm. The PCL group had a slightly higher average displacement of 145 μm and a larger standard deviation of 37.1 μm than the other groups during the first loading.

ANOVA results showed that there was no statistical difference between the two cemented groups, nor between the three press-fit cementless groups, as seen in Table 2. However, the cemented groups did have statistically significantly less micromotion than the cementless groups, which in turn had statistically less micromotion than the loose-fit cementless group. Because there was no statistical difference between the cementless groups HPF, PCC, or CPF, a recommendation of which cementless design is better cannot be made on the basis of micromotion.

Table 2: ANOVA results for the first loading cycle on LVDT data (α = 0.05)

Groups being compared	$\frac{F}{F_{crit}}$	*P*-value	Reject null hypothesis?
CON, HPF, PCC, CPF, MBC, PCL	12.20	4.65E-10	Yes
CON, MBC	4.05E-05	0.99	No
HPF, PCC, CPF, PCL	2.36	0.0021	Yes
HPC, PCC, CPF	0.059	0.80	No

As seen in Figure 6 and Table 3, the second loading cycle exhibited the same trend of correlation between cemented and cementless groups, but the average magnitudes were consistently lower than the first loading cycle. ANOVA results shown in Table 4 indicate that the displacements from the two loading cycles in the CPF, HPF and PCL groups were statistically different. This is most dramatic in the case of the PCL samples. The PCL group showed statistically more displacement from the other cementless groups for the first loading cycle but not for the second. It is theorized that the patella was significantly shifted from its preload position only during the first loading cycle, until the pegs were seated against the oversized holes. Since the patella was not disturbed between loading cycles, and the compressive load was applied in only one direction, the pegs were already settled against the side of the holes and had less room for movement.

Table 3: ANOVA results for the second loading cycle on LVDT data (α = 0.05)

Groups being compared	$\frac{F}{F_{crit}}$	*P*-value	Reject null hypothesis?
CON, HPF, PCC, CPF, MBC, PCL	7.70	5.11E-08	Yes
CON, MBC	0.016	0.78	No
HPF, PCC, CPF, PCL	0.17	0.66	No

Table 4: ANOVA results comparing the micromotion resulting from the first and second loading cycles (α = 0.05)

Group	$\frac{F}{F_{crit}}$	*P*-value	Reject null hypothesis?
CON	0.33	0.21	No
HPF	1.62	0.021	Yes
PCC	0.67	0.086	No
CPF	1.56	0.022	Yes
MBC	0.14	0.41	No
PCL	3.65	0.0023	Yes

The LVDT mounting arms as seen in Figure 4 were attached to the foam block approximately 2.4 cm below the top of the foam. This allowed for some compression of the foam, which can account for part of the displacement. Using the material property data for the rigid polyurethane foam block [30] and the dimensions between the top of the block and where the fixture was attached (approximately 5 cm × 5 cm × 2.4 cm), a compression of about 15 µm in the block can be calculated. To verify the material properties, a stress/strain curve was experimentally developed from a foam sample, as shown in Figure 7.

Using the experimentally determined elastic modulus and assuming a linearly elastic axially compressed member, the expected elastic micromotion is approximately 17 µm. The average normal and shear displacements are shown in Figure 8. The normal displacement could be reduced by 17 µm to account for the elastic deformation. Figure 7 also suggests that part of the difference in the first and second cycle loading displacements may be due to mechanical hysteresis of the foam material.

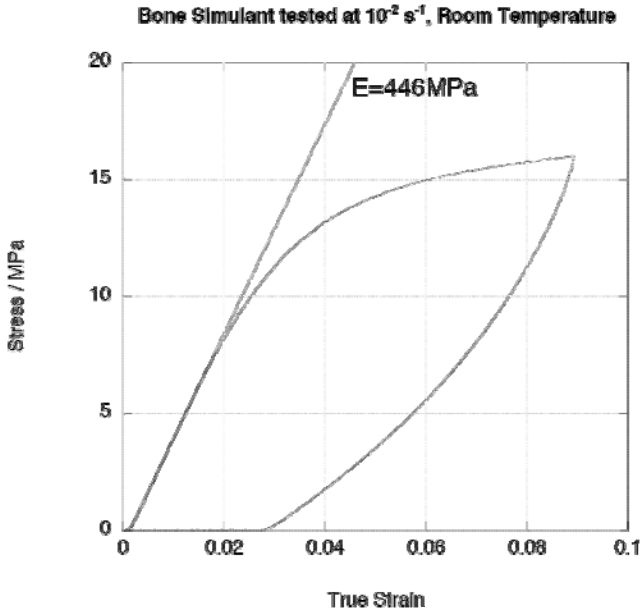

Figure 7: Stress-strain curve for foam material

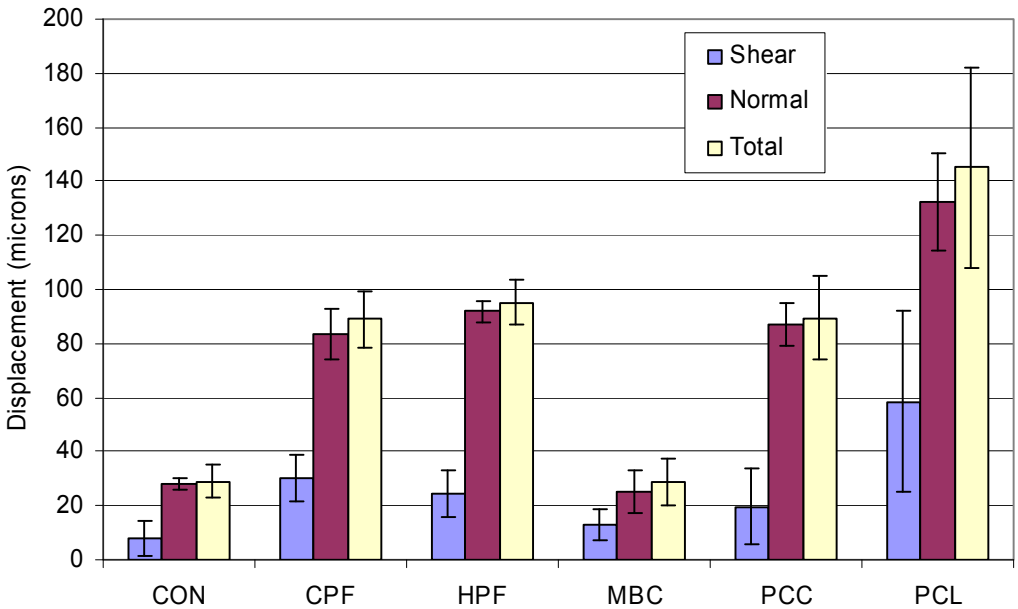

Figure 8: Maximum micromotion in the shear and normal directions during to the first loading cycle

3.2 Vibrations Test Evaluation

Initially, 15 samples were tested using both the LVDT and vibrations methods. A "natural variability" study was conducted to determine how much the testing procedure affected the results. Two different test samples were set up in the fixture. The entire testing procedure was followed to faithfully replicate the usual conditions as closely as

possible, including the testing duration, but the loading application was omitted. FRF and impedance readings were taken three times, corresponding to a measurement before the first loading cycle, in between loading cycles, and after the second loading cycle.

Comparisons of the reciprocity before, after, and between the loading cycles for the five different patella designs are shown in Figure 9. It was expected that the system would be linear before any loading is applied, and that the linearity would decrease after the first loading cycle, and even more so after the second. Only the CON group showed this expected behavior; the other groups suggest that as micromotion occurs, the system becomes more linear at some point. Figure 9 shows that there is no correlation between micromotion and reciprocity.

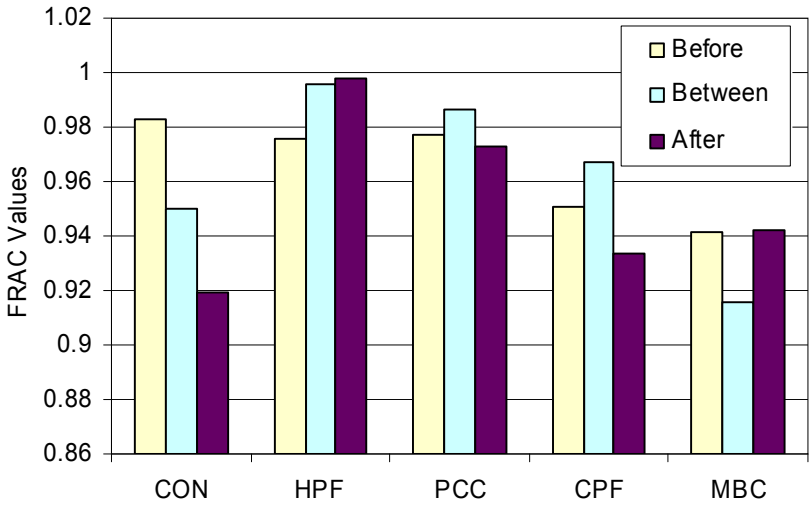

Figure 9: FRAC values for reciprocity tests

Figure 10 shows a comparison of an impedance result when no load is applied, that is the "natural variability" study, and one involving loading of a CPF sample. There should be no change between the three unloaded FRFs and impedance profiles if the vibrations methods accurately identified damage. Instead, the differences between profiles from the unloaded tests were of the same magnitude as the differences from the loaded tests, making it difficult to associate profile variability with either the inherent systematic noise or the actual structural deformation from the loading, as seen in Figure 10.

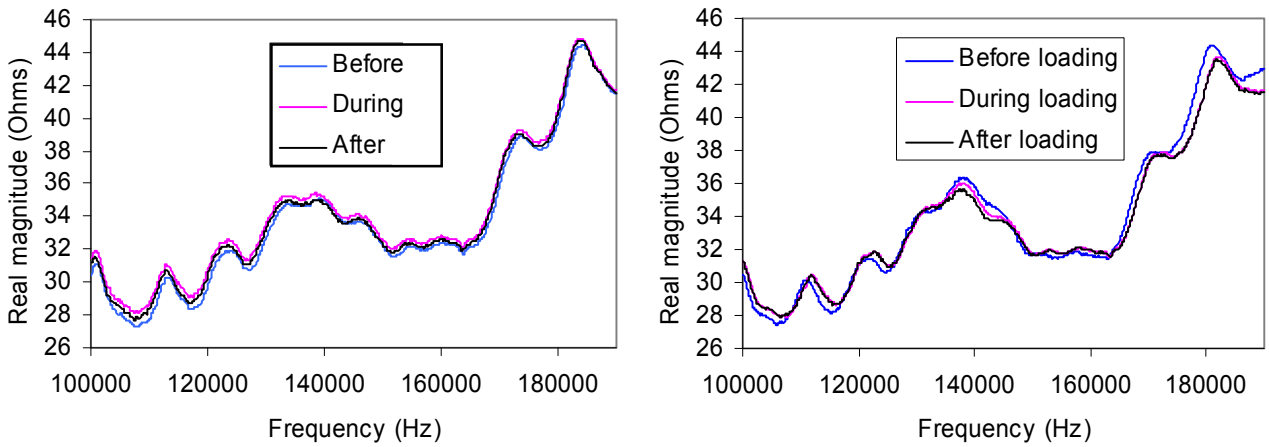

Figure 10: The impedance from the unloaded (left) CPF sample shows significant variability, on the order of the variability seen on the loaded sample (right)

The numerical analyses of the plots were as ineffective as the visual inspections. When comparing the differences in FRAC and cross-correlation between the initial and final impedance tests from each of the two patches on both samples, in four out of eight cases, the results implied more damage on the tests where loading was omitted. The analysis of the FRF data produced more optimistic results, as in each case, the damaged patellae had greater disturbance to the FRF than the undisturbed patellae. ANOVA results comparing CON, HPF, PCC, MBC, and CPF "before" and "during" data (when the most significant displacements occurred) are shown in Table 5, all using a significance level of $\alpha = 0.05$. It is clear that in each case, the null hypothesis cannot be rejected, and these tests do not show any statistically significant difference in the responses between the five groups.

Table 5: ANOVA vibrations results for the first loading cycle			
Test	$\frac{F}{F_{crit}}$	*P*-value	Reject null hypothesis?
FRF – FRAC	0.15	0.72	No
FRF – X-corr	0.15	0.72	No
Impedance (green patch) – FRAC	0.51	0.20	No
Impedance (green patch) – X-corr	0.52	0.20	No

When the best and worst performing samples from both types of vibrations tests were compared with those from the LVDT tests, it was clear that there were conflicting results. There appeared to be no correlation between the vibrations results and the actual micromotion measured from the LVDTs. Consequently, vibrations tests were excluded from the rest of the samples.

3.3 Sources of Uncertainty

As noted in Section 2.1, the CPF and HPF samples were designed to be inserted into bone drilled with an extra one millimeter inset circle. Since the rigid foam blocks did not have this inset accurately drilled, they were not able to distribute the shear stress in the way that they were designed, and instead, most of the load was carried by the pegs. It is possible that the results might have been different in these two groups had they been seated correctly. A new method of drilling the inset would need to be developed, as the inset circle would need to be aligned with the center of the peg hole pattern to a very tight tolerance.

Although the PCL group had a statistically larger displacement, the displacement was not as large as expected. As noted in Section 3.1, a compressive load was applied in a single direction. It is likely that changing the location of this load would result in significantly higher displacements for the PCL group, and to a lesser extent, for the other groups.

There are a few possible explanations for the ineffectiveness of the vibrations methods. The results were extremely sensitive to the position of the wires that connected the PZT patches and the data acquisition devices. In an attempt to suppress these undesirable effects, the wires were taped to stationary objects about 10 - 20 cm away from their connections at either end. Additionally, there was excessive noise from the vibrations of the loading machine. In an attempt to preserve consistent boundary conditions between tests, all vibrations tests were conducted with the test sample securely fastened in the loading fixture and the machine turned on. However, vibrations from the machine were of large enough magnitude to potentially affect the results.

3.4 Conclusions

The samples that exhibited the smallest micromotion were the cemented groups. All of the cementless groups had displacements that were at least twice as large as the cemented ones. However, due to the deformation of the foam block, the displacement measurements are conservative, with the projected displacement magnitudes about 15 μm -17 μm less than the results showed. Also, with the exception of the PCL group, all cemented and cementless test groups fell under the 150 μm threshold where fibrous tissue would start to develop, although the only two samples that met the < 40μm requirement for known osseointegration were the two cemented groups, CON and MBC. LVDT tests were found to be the most reliable method of measuring micromotion, as vibrations tests had too much natural variability to accurately assess mechanical stability on structures of this small scale.

4. Acknowledgments

This project was conducted as part of the Los Alamos Dynamics Summer School, which is part of the Los Alamos National Laboratory/University of California, San Diego Engineering Institute. Los Alamos National Laboratory provided funding for this project. The following companies generously provided the software for the summer

school: Vibrant Technologies (MEScope experimental modal analysis software), The Mathworks, Inc. (MATLAB numerical analysis software, Simulink, and XPCTarget), and ABAQUS, Inc. (ABAQUS finite element software). The authors would like to thank Mohamed Soliman and Stryker Orthopaedics for their support of this project.

REFERENCES

[1] Baech, J. and H. Kofoed, *Failure of metal-backed patellar arthroplasty. 47 AGC total knees followed for at least 1 year.* Acta Orthop Scand, 1991. **62**(2): p. 166-8.

[2] Piazza S J, Moran M F, Okita N, Landon R. Biomechanical assessment of micromotion in cementless femoral components in total knee replacement. Preliminary report, 2005.

[3] Lee, T.Q., S.L. Barnett, and W.C. Kim, *Effects of screw types in cementless fixation of tibial tray implants: stability and strength assessment.* Clin Biomech (Bristol, Avon), 1999. **14**(4): p. 258-64.

[4] Sala, M., M. Taylor, and K.E. Tanner, *Torsional stability of primary total knee replacement tibial prostheses: a biomechanical study in cadaveric bone.* J Arthroplasty, 1999. **14**(5): p. 610-5.

[5] Stern, S.H., R.D. Wills, and J.L. Gilbert, *The effect of tibial stem design on component micromotion in knee arthroplasty.* Clin Orthop Relat Res, 1997(345): p. 44-52.

[6] Bai, B., et al., *Effect of posterior cut angle on tibial component loading.* J Arthroplasty, 2000. **15**(7): p. 916-20.

[7] Kraemer, W.J., I.J. Harrington, and T.C. Hearn, *Micromotion secondary to axial, torsional, and shear loads in two models of cementless tibial components.* J Arthroplasty, 1995. **10**(2): p. 227-35.

[8] Lee, R.W., R.G. Volz, and D.C. Sheridan, *The role of fixation and bone quality on the mechanical stability of tibial knee components.* Clin Orthop Relat Res, 1991(273): p. 177-83.

[9] Lee, T.Q., S.L. Barnett, and W.C. Kim, *Effects of screw types in cementless fixation of tibial tray implants: stability and strength assessment.* Clin Biomech (Bristol, Avon), 1999. **14**(4): p. 258-64.

[10] Sala, M., M. Taylor, and K.E. Tanner, *Torsional stability of primary total knee replacement tibial prostheses: a biomechanical study in cadaveric bone.* J Arthroplasty, 1999. **14**(5): p. 610-5.

[11] Stern, S.H., R.D. Wills, and J.L. Gilbert, *The effect of tibial stem design on component micromotion in knee arthroplasty.* Clin Orthop Relat Res, 1997(345): p. 44-52.

[12] Yoshii, I., et al., *The effect of central stem and stem length on micromovement of the tibial tray.* J Arthroplasty, 1992. **7 Suppl**: p. 433-8.

[13] Browne, C., et al., *Patellofemoral forces after total knee arthroplasty: effect of extensor moment arm.* Knee, 2005. **12**(2): p. 81-8.

[14] Hsu, H.P. and P.S. Walker, *Wear and deformation of patellar components in total knee arthroplasty.* Clin Orthop Relat Res, 1989(246): p. 260-5.

[15] Miller, R.K., et al., *In vitro measurement of patellofemoral force after three types of knee replacement.* J Bone Joint Surg Br, 1998. **80**(5): p. 900-6.

[16] Petersilge, W.J., et al., *The effect of trochlear design on patellofemoral shear and compressive forces in total knee arthroplasty.* Clin Orthop Relat Res, 1994(309): p. 124-30.

[17] Singerman, R., J. Berilla, and D.T. Davy, *Direct in vitro determination of the patellofemoral contact force for normal knees.* J Biomech Eng, 1995. **117**(1): p. 8-14.

[18] Singerman, R., et al., *A six-degree-of-freedom transducer for in vitro measurement of patellofemoral contact forces.* J Biomech, 1994. **27**(2): p. 233-8.

[19] Singerman, R., et al., *Patellar contact forces with and without patellar resurfacing in total knee arthroplasty.* J Arthroplasty, 1999. **14**(5): p. 603-9.

[20] Singerman, R., et al., *Effect of femoral component rotation and patellar design on patellar forces.* Clin Orthop Relat Res, 1997(334): p. 345-53.

[21] Zavatsky, A.B., P.T. Oppold, and A.J. Price, *Simultaneous in vitro measurement of patellofemoral kinematics and forces.* J Biomech Eng, 2004. **126**(3): p. 351-6.

[22] Kaiser, A.D. and L.A. Whiteside, *The effect of screws and pegs on the initial fixation stability of an uncemented unicondylar knee replacement.* Clin Orthop Relat Res, 1990(259): p. 169-78.

[23] Miura, H., et al., *Effects of screws and a sleeve on initial fixation in uncemented total knee tibial components.* Clin Orthop Relat Res, 1990(259): p. 160-8.

[24] Singerman, R., et al., *Effect of tibial component position on patellar strain following total knee arthroplasty.* J Arthroplasty, 1995. **10**(5): p. 651-6.

[25] Bragdon, C.R., et al., *Differences in stiffness of the interface between a cementless porous implant and cancellous bone in vivo in dogs due to varying amounts of implant motion.* J Arthroplasty, 1996. **11**(8): p. 945-51.

[26] Engh, C.A., et al., *Quantification of implant micromotion, strain shielding, and bone resorption with porous-coated anatomic medullary locking femoral prostheses.* Clin Orthop Relat Res, 1992(285): p. 13-29.

[27] Pilliar, R.M., J.M. Lee, and C. Maniatopoulos, *Observations on the effect of movement on bone ingrowth into porous-surfaced implants.* Clin Orthop Relat Res, 1986(208): p. 108-13.

[28] Soballe, K., et al., *Tissue ingrowth into titanium and hydroxyapatite-coated implants during stable and unstable mechanical conditions.* J Orthop Res, 1992. **10**(2): p. 285-99.

[29] Park, G,. et al., *Piezoelectric Active Sensor Self-Diagnostics Using Electrical Admittance Measurements*. Journal of Vibrations and Acoustics, 2006(128): p. 469-76.

[30] Pacific Research Laboratories, 2007, Solid Rigid Polyurethane Foam, http://www.sawbones.com/products/bio/testblocks/solidfoam.aspx (July 31, 2007)